Journal of Magnetic Resonance 300 (2019) 103–113

Contents lists available at ScienceDirect

Journal of Magnetic Resonance

journal homepage: www.elsevier.com/locate/jmr

Framework for and evaluation of bursts in random sampling of multidimensional NMR experiments

Mehdi Mobli *, Tomas M. Miljenović

Centre for Advanced Imaging, The University of Queensland, St. Lucia, QLD 4072, Australia

ARTICLE INFO

Article history:
Received 23 November 2018
Revised 23 January 2019
Accepted 24 January 2019
Available online 26 January 2019

Keywords:
Nonuniform sampling
Multidimensional NMR
Burst sampling
Clustered sampling
Sampling
Exponentially weighted sampling
Jittered sampling

ABSTRACT

The grouping of data in bursts, also referred to as clusters, spikes or clumps, is a common phenomenon in stochastic sampling. There have been several reports that suggest that in NMR, the presence of such bursts is beneficial to spectral reconstruction where data are sampled nonuniformly. In this work, we seek to define a mode of sampling that produces bursts of randomly distributed data in a controlled manner. An algorithm is described for achieving this where the burst length and its uniformity is controlled – we refer to this type of sampling mode as clustered sampling. Measures are introduced for assessing the "burstiness" of nonuniformly sampled data in multiple dimensions and properties of the point-spread-function of these schedules are assessed. The clustered sampling method is applied to samples drawn from an exponentially weighted distribution either distributed randomly or pseudo-randomly by use of a jittering algorithm. The results reveal that bursts introduce characteristic sampling artifacts that are shifted to low frequencies (red shifted), with respect to the signal frequency, and that they produce artifact-reduced regions at frequencies related to the burst length. This observation is contrary to that observed for sampling methods that seek to evenly distribute NUS data, such as jittered or Poisson sampling. Extensive evaluation of simulated data with comparable inherent sensitivity, reveals that at high sampling coverage (25% in 1D), the distribution of the data has little impact on common spectral quality measures. Application of the introduced clustered sampling method to an experimental 3D NOESY experiment showed results consistent with that found for the simulated 1D data. However, in the extremes of very sparse sampling, the results suggest that there may be some advantages associated with incorporation of bursts in nonuniform sampling. The tools and theory presented will serve as a starting point to further explore this novel mode of sampling in NMR.

1. Introduction

Nonuniform sampling (NUS) in multidimensional NMR is a powerful method for improving the resolution and sensitivity of lengthy experiments [1]. The selected sample points are typically drawn from a probability density function (PDF) that mimics the signal envelop to improve sensitivity per unit time of data acquisition [2]. The samples are selected stochastically from this distribution to minimize coherence that would otherwise result in strong sampling artifacts (aliasing in the extreme case) [3]. Most recently NUS has been augmented by various methods to generated pseudo-random distributions, where the distance between adjacent points is controlled by either defining regions of equal probability, from which samples are selected using jittering (also named quantile sampling) [4,5] or by imposing constraints on the "gap" between samples, e.g. Poisson-gap sampling [6,7]. These pseudo-random methods have the benefit of producing distributions of samples that are less sensitive to the random seed used to generate them, whilst also providing a more uniform coverage of the sample space. These properties are desirable as they ensure that data samples are not chosen that have an extreme distribution (i.e. selection of the first or last "*m*" points or every other point).

There have also been efforts to find additional gains in sensitivity by use of prior knowledge about the signal frequencies. An implementation of this known as the "beat matched sampling" (BMS) method biases the sampling based on the known chemical shift of the signals [8]. A thorough analysis of BMS, however, found only modest gains in sensitivity with reduced robustness com-

Abbreviations: EJS, exponentially-weighted jittered sampling; ERS, exponentially-weighted random sampling; PDF, probability density function; PSR, peak-to-sidelobe ratio; PSF, point-spread-function; NUS, nonuniform sampling.

* Corresponding author.
E-mail address: m.mobli@uq.edu.au (M. Mobli).

https://doi.org/10.1016/j.jmr.2019.01.014
1090-7807/

pared to selection of samples from a PDF based solely on the signal decay envelope.

Separate to these efforts, work has been undertaken to identify NUS distributions that produced spectral reconstructions with the "best" properties [9]. This work found that "bursty" distributions resulted in particularly favorable reconstructed spectra. Since this study, there have been no systematic evaluation of the effects of "bursts" as a method of improving spectral qualities from NUS data. The use of the term "burst sampling" has however occurred when discussing augmentation of sine-weighted Poisson gap sampling, triangular backfilling in quantile sampling and also applied to cases where blocks of time-domain data are acquired for reconstruction [5,6,10]. In these cases, specific forms of bursts of samples are used (triangles/sine-burst gap/blocks) without a systematic evaluation of the consequences of introducing such bursts.

Here, we wish to explore burst sampling in a more systematic way. First, the distinction is made that our approach can be viewed as sampling in clusters – defined as groups of adjacent points with a defined length along each dimension of a multidimensional object – where the outcome is "bursty" data. The distinction is made as burstiness is a property of the sampling schedule, and not necessarily a well-defined method of sampling. For example, the original description of burst sampling in NMR was an observation that some randomly generated sequences were bursty, but these were not sampling schedules that had been generated using a particular algorithm to produce this behaviour. Thus, although any sampling schedule may be bursty, the clustered sampling method presented here will generate sampling schedules that have a bursty appearance by design.

Based on the above, our framework needs to define (i) the length of each burst and (ii) how many samples to draw from each burst. This allows us in the first instance to address the question of (a) what happens to the PSF as the burst length is increased and (b) how does this gradually break down as we sample nonuniformly within each burst (reducing the overall burstiness of any particular schedule). The aim is to provide insights into the consequences of bursts of NUS samples and explore if any measurable gains can be achieved. Finally, we will combine our clustered sampling method in a general way with a weighted random sampling method (exponential random sampling) and a weighted pseudo-random sampling method (jittered sampling).

2. Theory and methods

All of the presented data were generated and processed using the Rowland NMR toolkit (*RNMRTK, available from UConn Health Centre*) unless otherwise stated. The experimental NMR data presented was measured (by Topspin) using a 300 μM sample of uniformly ^{13}C and ^{15}N labelled VST×1 (a 4 kDa potassium channel inhibitor), recorded as part of a previous study using a cryoprobe equipped Bruker instrument operating at a ^{1}H frequency of 900 MHz [11].

2.1. The clustered sampling method

The clustered sampling method is here presented using the previously described one-pass method implemented for NUS in multidimensional NMR for up to 3 dimensions [4,12]. The theory of this method has been previously described in detail including its extension for jittered sampling [4], and will here only be described in brief. First, an L dimensional grid is created (Nyquist grid hereafter), with each dimension having T_k points (along the k^{th} dimension). The total size of the grid (N) is defined by the product of the number of points along each dimension:

$$N = \prod_{k=1}^{L} T_k \tag{1}$$

The probability ($p(i)$) associated with each point (i) on the Nyquist grid is calculated based on the desired PDF, i.e. exponential decay for regular NMR acquisition:

$$p(i) = \prod_{k=1}^{L} e^{-i\pi lw_k/sw_k} \tag{2}$$

where lw_k and sw_k are the linewidth and spectral window in the k^{th} dimension, respectively, and the equation may be further augmented to include, for example, J modulation. Then a rank is calculated for each point $r(i)$ according to:

$$r(i) = x(i)^{1/p(i)} \tag{3}$$

where $x(i)$ is a random number between 0 and 1. The rank $r(i)$ is then sorted in descending order. The number of points, subsampled from N, is defined as m, where $m \leq N$. The top m points represent random points from the defined exponential distribution – this approach involves only the sorting (or ranking) of $r(i)$ after the PDF is defined to generate the requested random samples with the defined weighting and is therefore referred to as a "one-pass" method. When samples are selected from an exponentially decaying PDF according to the ranks of Eq. (3), it is referred to here as exponential random sampling (ERS).

The algorithm has been adapted for jittered sampling, where the PDF is divided into equiprobable regions (or quantiles/percentiles) [4]. Samples are drawn from each region based on the rank in Eq. (3). This method is similar to the quantiles method recently described [5], with the distinction that the regions do not adhere to rectangular shapes but instead adhere strictly to being equiprobable by augmenting the shape of the equiprobably regions on the underlying PDF.

Perhaps, the simplest approach to implementing burst sampling is to define a region of adjacent points as a "cluster" of samples with a geometry defined by the length of the cluster along each dimension (k), c_k, and to use this value to increase the grid spacing by taking the quotient $\frac{sw_k}{c_k}$ for each dimension k, and similarly reducing the number of samples to be drawn by $\frac{T_k}{c_k}$ for each dimension k. Once the reduced samples are selected from the augmented grid, the samples are extended to c_k for each dimension. This approach, however, introduces an additional level of order, such that a cluster can only start at regular intervals. I.e. if two-point clusters are sought, all clusters will lie on a sub grid that starts with either even or odd numbered coordinates – depending on how the grid is initiated.

Thus, an alternative method was developed where each coordinate on the Nyquist grid initiates a cluster of length c_k, for each dimension k. Thus, given a grid of size T_k there will be:

$$C = \prod_{k=1}^{L} T_k - [c_k - 1] \tag{4}$$

clusters to be considered (where C is the total number of clusters). For each cluster the average rank (Eq. (3)) of all points in that cluster is also computed. The clusters are then sorted based on their rank, and the top ranked cluster is chosen. Subsequent clusters are evaluated in order of rank and discarded if they overlap with existing clusters. The procedure is repeated until all clusters are evaluated or m points have been selected.

Visually the procedure can be considered as applying a mask of a given length along the different dimensions. For example, if clustering according to pairs is sought along two dimensions, a 2×2 mask is generated, originating from every point where the mask does not exceed the boundaries of the grid. Geometrically, the

mask will be a rectangle in 2D and a cube in 3D. The masks will naturally overlap and overlapping masks are eliminated according to the above procedure during the selection step.

The described method will allow for schedules according to Fig. 1B and C to be produced for an arbitrary number of dimensions and cluster length (c_k). To decrease the uniformity of the clusters the following procedure is implemented where a fraction (f) of m is rejected as described.

(1) The value of m is multiplied by the requested fraction f and rounded to the nearest integer: $m' = m(1 + (\prod c_k - 1)f)$.
(2) After the above selection procedure, m' points are selected, the difference between m' and m is calculated and the resulting number of samples are removed randomly, $\Delta = m' - m$.

When $f = 0$, no samples are removed and when $f = 1$, $m(c_k - 1)$ samples are removed. As an example, if $c_k = 3$ (as in the case in Fig. 1C), then setting $f = 0$ has no effect on the selection or clustering, whilst setting $f = 1$, results in removing two out of every three data points selected after step (5) of the algorithm (Fig. 1D). This is constructed, such that setting $f = 1$ drives the sampling close to random sampling (Fig. 1A). It should be noted that even when $f = 1$ the samples being rejected are still from a clustered set of samples and will therefore retain some of the properties of the original clustered selection. Values of f between 0 and 1 will linearly introduce increasing levels of disorder to the clusters.

The following nomenclature is used here for clustered sampling. The value of c_k is used as a superscript before c_k and the value of f is used a subscript to letter "f" denoting random rejection. Two-point clusters are hence indicated by: ^2c, and where the clustering coherence is reduced through random rejection using a value of $f = 0.5$, this is indicated as $^2cf_{0.5}$.

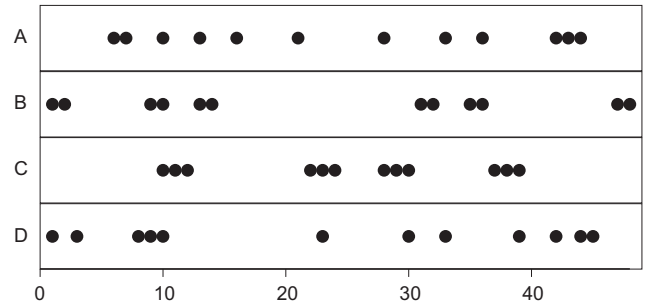

Fig. 1. Nonuniformly sampled data with and without bursts (dots are shown where a sample is taken and omitted where one is not taken). In each case 12 samples are taken from a grid of 48 samples. The distribution is according to: (A) random samples, (B) random samples with 2-point bursts, (C) random samples with 3-point bursts and (D) random samples of 3-point bursts with random rejection.

In order to apply clustered sampling where the data are also distributed evenly based on the underlying probability density, a variant of the previously described jittered sampling method is used here [4]. In this implementation, once the algorithm reaches the stage of comparing clusters to find overlapping clusters, it will additionally exclude any clusters that belong to a jittered region that has previously been sampled (all of the points must belong to previously sampled regions). It should be noted that in this implementation, if the number of jitter-regions is set to the number of clusters specified (m/c_k), the dual constraints for rejection (overlapping clusters and jitter-regions), results in retention of fewer samples than specified. The constraints can be relaxed by increasing the number of jittered regions. The factor by which the number of regions needs to be expanded was empirically determined (jitter-regions $= m/\alpha c_k$, where α is set to 0.8). The above sampling methods are incorporated into the latest version of the sched3d software (sched3d6), available via the NMRBox project [13].

We also note that the clustering procedure will augment the PDF. Thus, it is more pertinent to empirically select PDFs that are, based on a suitable metric, comparable to that of a weighted PDF with well-defined characteristics [4,6]. This is done here (as previously [4]) using the following measure of the inherent sensitivity of a sampling schedule:

$$R'(\boldsymbol{K}) = \frac{N}{m}\frac{\sum_{i=1}^{N} k_i p_i}{\sum_{i=1}^{N} p_i} \tag{5}$$

where $\boldsymbol{K}$ is the sampling function, k_i has the value 1 for sampled times and zero for times not sampled and p_i is as defined in Eq. (2). Note that Eq. (5) was adjusted [4] from its original form [14] to scale for the number samples selected from a pre-defined Nyquist grid.

2.2. A measure of "burstiness"

In the above section a method is introduced for generating "bursty" sampling schedules. The same principle can be used to define a measure of "burstiness". Here we have written an algorithm that uses the above described "masking" method to search for multiple adjacent samples.

Sample-wise "burstiness" is determined by occupancy within a particular $\gamma_1 \times \gamma_2 \times \cdots \times \gamma_L$, L-orthotope, or "mask" (M). $B_M(j)$– the burstiness score for a sample j, given a mask M – is the maximum number of samples that can be contained within a region of shape and orientation M that also includes j, normalised by the volume of M (Fig. 2).

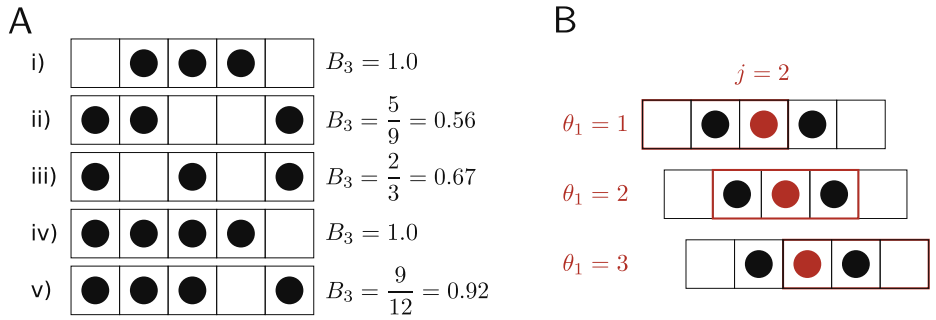

Fig. 2. B_3 burstiness values for undersampled Nyquist grids. In each case, samples were selected from a Nyquist grid containing only 5 points; dots are shown where a sample is taken, and omitted where one is not taken. In section A), B_3 values are shown for five different sampling schedules (i-v). In section B), schedule i) is used to demonstrate the calculation of a burst density for a particular sample. The burst mask M, with origin point θ_1, is indicated in red; the sample density is highest when $\theta_1 = 2$, and resulting burst density for the sample is $B_3(j) = 3 \div 3 = 1$. Note that the samples on either end of the burst, have the same sample-wise "burstiness" score as the central point.

As mentioned earlier, there does not appear to be a current consensus as to how many samples, measured at which particular sampling rate (or with a given sample separation) constitutes a "burst". Further, we reasoned that any measure may require per-dimension weighting when evaluating burstiness for some higher-dimensionality schedules. (Varying mask dimensions even allows for burstiness to only be measured for a particular dimension, by setting $\gamma_k = 1$ for all other dimensions.) Therefore, while we recommend using a mask with length $\gamma_k = 3$ for each dimension by default, our measure allows for these parameters to be adjusted. Given these reasons, any burstiness value determined using our method should be reported together with the mask shape – even if our recommended values are used.

Our measure evaluates the "burstiness" of a sampling schedule, by calculating the maximum "burstiness" score for each individual sample ($B_M(j)$) and reporting the mean result:

$$B_M = \sum_{j=1}^{J} \frac{B_{\gamma_1 \times \gamma_2 \times \ldots \times \gamma_L}(j)}{J} = \overline{B_M(j)} \tag{6}$$

A more comprehensive description of our burstiness measure is as follows:

(1) A sampling schedule (1-indexed) is taken as input.
(2) The input schedule is used to create a minimal Nyquist grid N, containing all points in the schedule and using the schedule's grid spacing. This is achieved by
  (I) determining the dimensionality (L) of the schedule;
  (II) constructing an L-dimensional zero matrix,[1] which has $T_k = max(j_k)$ points in each dimension;
  (III) setting $N(j) = 1$, for each sample co-ordinate j contained in the schedule.
(3) Sample by sample, the region around each point j is examined to determine a localised value of "burstiness":
  (I) define an L-dimensional "burst mask" M, with dimensions $\gamma_1 \times \gamma_2 \times \ldots \times \gamma_L$ and thus $J = \prod_{k=1}^{L} \gamma_k$ elements (see below);
  (II) for each point j in the sampling schedule, perform a geometric check to evaluate how "bursty" the schedule is in each direction (up to γ_k points away, along each dimension):
  (i) define all possible origin points $(\theta_1, \theta_2, \ldots, \theta_L)$ for an M-sized region, which would contain the point j and fall within the bounds of N:
    (1) beginning with $(\theta_1, \theta_2, \ldots, \theta_L) = (j_1 - \gamma_1 + 1, j_2 - \gamma_2 + 1, \ldots, j_L - \gamma_L + 1,)$, check all j possible co-ordinates satisfying $\theta_k \in [i_k - \gamma_k + 1, i_k]$;
    (2) remove any origin points containing ordinate $\theta_k < 0$ or $\theta_k + \gamma_k > T_k$.
  (ii) for each remaining origin point, take an M-sized slice from N;
  (iii) calculate a sample density for that particular slice, by summing all elements and dividing by J.
  (III) retain the largest value sample density value as $B_M(j)$, the maximum "burstiness" of sample point j (for a given burst mask M).
(4) Determine a mean burstiness value $B_M = \overline{B_M(j)}$ for the entire schedule.

The reference implementation of the algorithm was coded in Rust (http://rust-lang.org). The *ndarray* (https://github.com/bluss/ndarray) crate was used to facilitate a more geometric implementation for arbitrary values of L for easier debugging, while still retaining sufficient performance. The implementation is available via the NMRBox project.

[1] *Or, as per our implementation, a more computationally-efficient equivalent.*

2.3. Peaky – a peak-picking algorithm for the Rowland NMR toolkit

An automated peak picking and model fitting algorithm was written for the Rowland NMR toolkit, called *Peaky*. The algorithm sets a threshold based on the noise level in the spectrum and identifies local maxima. Adjacent maxima are grouped together. Each group is then fitted to a mixed Gaussian/Lorentzian lineshape using a Levenberg-Marquardt non-linear least squares approach (LM library from MINPACK [15]). The data are fitted to the amplitude, frequency, line-width and a Gaussian/Lorentzian weighting factor β (three additional parameters per added dimension). The algorithm further is able to resolve overlapped peaks using the minimum descriptive length (MDL) criterion previously described [16]. The algorithm either uses an input noise threshold for peak picking, or adjusts the threshold for peak picking until a user-defined number of signals is detected (the algorithm seeks to find at least half as many as the requested signals, but no more than twice the requested signals by adjusting the threshold). The algorithm can accept up to 4D data and was tested rigorously in-house for 1D data. The software is available via NMRBox, where further details and the test data are available.

3. Results

3.1. Bursts in 1D

The effect of introducing bursts of samples through the above clustered sampling method was evaluated by generating synthetic data. First, the behaviour of the PSF was assessed by subsampling 128 data points from a 512 point Nyquist grid (all spectral parameters selected as described previously [4]).

A critical aspect of impartial comparison of two methods of generating sampling schedules (according to different distributions) involves ensuring that the relative sensitivity of two sampling schedules are comparable when performing any assessment. It is only under these conditions that it is possible to assess whether the distribution of the data (and not the intrinsic sensitivity of the sampled data) is responsible for any differences found when comparing different sampling methods. Here, we will generate sampling schedules that have a distribution equivalent to that of the decay envelope produced by a Lorentzian signal with a 10 Hz linewidth. The one-pass method has previously been shown to produce distributions that reproduce the exponential weighting of the PDF, however, methods such as jittered and Poisson-gap sampling or augmentation by sine-weighting will result in schedules that have distributions that deviate from the ideal distribution. To ensure that the schedules generated using the jittering or clustered sampling methods are of comparable sensitivity, we will compare the $R'(\boldsymbol{K})$ value of these schedules with those obtained when using the one-pass method noted above [4]. This procedure is performed empirically on a small set of sampling schedules (1 0 0) prior to generating the schedules used for the more detailed statistical analysis (1000 sampling schedules with different random deviates).

The following sampling methods were evaluated. Random sampling with an exponentially weighted PDF having a decay parameter (T_2 = 0.032 s) corresponding to frequency domain signal with a *lw* (i.e. full width at half maximum) of 10 Hz (ERS). The clustered sampling method was used to generate bursts of two and three adjacent points, the former with random rejection using a value of $f = 0.25, 0.5, 0.75$ (i.e. ${}^2c$, ${}^3c$ and ${}^2cf_{0.25}$, ${}^2cf_{0.5}$, ${}^2cf_{0.75}$ –

according to nomenclature introduced in theory and methods section). A series of schedules were also generated combining jittered sampling with an exponentially weighted PDF, focused on bursts of length = 2 (^2c, and $^2cf_{0.25}$, $^2cf_{0.5}$).

$R'(\boldsymbol{K})$ was computed for 100 schedules with the parameters described above. The *lw* parameter was adjusted for the clustered sampling methods to arrive at the same $R'(\boldsymbol{K})$ value as the ERS schedule to aid comparisons. Table 1 contains statistics regarding the distribution of data in the sampling schedules generated.

The value of $R'(\boldsymbol{K})$ is, as expected, constant within the statistical error, and as previously established there is less seed-dependent spread of this metric for the jittered methods compared to the random sampling methods [4]. The narrow range of various schedule-statistics for jittered sampling is reduced as random rejection is introduced in the clustered-sampling methods. Finally, the burstiness measure was evaluated for all 1000 sampling schedules, evaluating the measure for burst lengths of 2 and 3. The data show that random sampling is inherently more bursty than jittered sampling, and that the random rejection method reduces the burstiness of the clustered sampling method.

For each of the schedules, a PSF was generated by setting the values of the data points not sampled to zero, and computing the DFT. In Fig. 3, representative examples of the PSFs of each sampling method are displayed in magnitude mode. The general trend is that the bursts result in increased artifacts near the base of the 0-(Hz)-frequency signal, and significantly reduces artifacts at a position in the PSF related to the burst length. This red-shifted noise is the opposite of the blue shift seen in PSFs of Poisson-based and jittered sampling [4,17].

Statistics relating to the distribution of the data in the PSF were calculated as previously described [4] and are presented in Table 2. The data show that the amplitude of the highest artifact (in relationship to the 0-frequency component) increases for burst lengths of two or three, while introducing the random rejection methods, effectively counteracts this increase, driving the statistics closer to random sampling.

3.2. Performance on synthetic data

The *Peaky* algorithm allows us to interrogate whether the distribution of sampling artifacts is particularly beneficial in spectral data generated from any of the sampling methods tested here. This was done by simulating an FID with seven signals with decreasing amplitudes. The Nyquist grid was constructed using the same parameters as those described above for the PSF data. All synthetic peaks were generated by the *Lorentz* command in *RNMRTK*. The most intense signal was defined as having an amplitude of 10, and each subsequent signal had 0.5 subtracted from their amplitude, providing a range of amplitudes from 10 to 7 (the range was determined such that the weakest peak would be close to

Table 1
Summary of statistics describing the distribution of sampling points when using different sampling methods. Note that the exponential weighting parameter (lw) was varied to achieve the same $R'(\boldsymbol{K})$ value. Average and median of the sampling coordinates are reported as a fraction of the longest evolution time (512). Burstiness is calculated as described in the text with burst lengths of 2 and 3 evaluated. The different sampling methods are described by the nomenclature introduced in the theory and methods section. ERS: exponentially-weighted random sampling, ERS ^2c: exponentially-weighted random sampling in bursts of length 2, ERS ^3c: exponentially-weighted random sampling in bursts of length 3, EJS: exponentially-weighted jittered sampling, EJS ^2c: exponentially-weighted jittered sampling in bursts of length 2, EJS $^2cf_{0.5}$: exponentially-weighted random sampling in bursts of length 2 with random rejection of half the data (see text for detailed definition).

	$R'(K)$		A_{ev}		M_{ev}		Burstiness	
	Av	St. dev.	Av	St. dev.	Av	St. dev.	B_2	B_3
ERS	1.45	5.2E−02	0.324	1.8E−02	0.263	2.4E−02	0.79	0.69
ERS ^2c	1.45	6.3E−02	0.324	2.3E−02	0.265	2.9E−02	1.00	0.80
ERS $^2cf_{0.25}$	1.45	5.7E−02	0.324	2.1E−02	0.267	2.6E−02	0.92	0.75
ERS $^2cf_{0.5}$	1.45	5.4E−02	0.322	2.0E−02	0.268	2.4E−02	0.89	0.71
ERS $^2cf_{0.75}$	1.44	5.0E−02	0.319	1.8E−02	0.271	2.2E−02	0.83	0.70
ERS ^3c	1.45	7.6E−02	0.324	2.8E−02	0.265	3.5E−02	1.00	1.00
ERS $^3cf_{0.25}$	1.45	5.7E−02	0.320	2.1E−02	0.268	2.5E−02	0.91	0.82
EJS	1.45	5.0E−04	0.324	2.5E−04	0.258	1.6E−03	0.64	0.54
EJS ^2c	1.44	3.0E−02	0.325	7.9E−03	0.265	1.3E−02	1.00	0.75
EJS $^2cf_{0.25}$	1.45	3.8E−02	0.324	1.2E−02	0.265	1.8E−02	0.91	0.69
EJS $^2cf_{0.5}$	1.45	4.4E−02	0.321	1.4E−02	0.262	2.0E−02	0.88	0.69

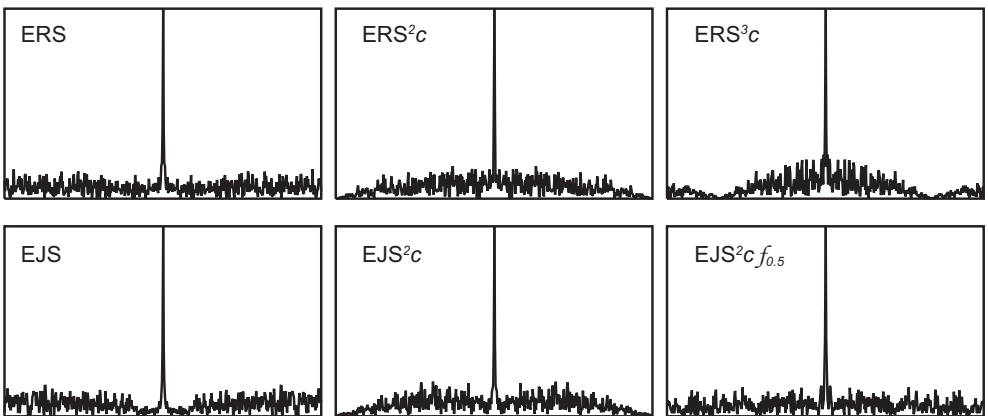

Fig. 3. Point-spread-function of various nonuniform sampling methods, where the method is noted in the top-left corner of each spectrum. See theory and methods section or Table 1 heading for details of abbreviations used.

Table 2
Summary of statistics related to point-spread-function of sampling methods evaluated. The peak-to-sidelobe ratio (PSR) is reported in each case as well as the distribution of sampling noise as measured by the mean of the l_1-norm ($\overline{M}_{PSF}$) and the variance (σ_{PSF}) of this value. See text or Table 1 heading for details of abbreviations used.

	PSR		$\overline{M}_{PSF}$		σ_{PSF}	
	Av	St. dev.	Av	St. dev.	Av	St. dev.
ERS	5.74	0.55	0.51	1.1E−02	0.27	1.1E−02
ERS ^2c	5.06	0.53	0.46	1.1E−02	0.32	1.2E−02
ERS $^2cf_{0.25}$	5.33	0.54	0.49	1.1E−02	0.28	1.2E−02
ERS $^2cf_{0.5}$	5.55	0.57	0.50	1.0E−02	0.27	1.2E−02
ERS $^2cf_{0.75}$	5.69	0.55	0.50	1.0E−02	0.27	1.1E−02
ERS ^3c	4.42	0.51	0.42	1.1E−02	0.35	1.5E−02
ERS $^3cf_{0.25}$	5.29	0.59	0.49	1.1E−02	0.28	1.3E−02
EJS	5.12	0.54	0.52	5.6E−03	0.29	9.7E−03
EJS ^2c	4.78	0.50	0.48	6.5E−03	0.34	8.9E−03
EJS $^2cf_{0.25}$	5.16	0.53	0.50	8.5E−03	0.29	1.1E−02
EJS $^2cf_{0.5}$	5.44	0.55	0.51	9.3E−03	0.28	1.1E−02

the sampling noise level at the level of NUS investigated). All signals were modeled with a decay equivalent to a linewidth of 10 Hz (to match the decay in the sampling schedules). The signals were further not allowed to be closer than 100 Hz of each other, to avoid confounding issues of overlap. Noise was added to the FID (with a standard deviation of 1.2), such that the weakest signal had an S/N of ∼50 in the DFT of the linearly sampled FID (512/512). This would ensure that, in the absence of a PSF deconvolution algorithm (i.e. maximum entropy reconstruction (MaxEnt), iterative soft thresholding (IST), compressed sensing (CS) etc.), the DFT of the zero-augmented data (referred to hereafter as nuDFT) would be dominated by sampling artifacts. To evaluate the contribution of the sampling artifacts (rather than a spectral reconstruction algorithm), the nuDFT spectrum was used in the subsequent peak analysis step.

To also interrogate the variation in the sampling artifacts due to the distribution of the signals, the frequencies of the signals were randomly varied for each of the seven signals for each of the 1000 sampling schedules generated above. Although this results in co-variation of two variables (random seed used to generate the sampling schedule and frequency of synthetic signals), the size of the dataset should provide sufficient redundancy to draw meaningful conclusions on the performance of each sampling method.

Peaky was initiated by requesting 14 signals, this ensures that at least seven signals are identified, these may or may not be the injected signals depending on the level of interference from the sampling artifacts. Thus, it is possible to perform an analysis similar to the previously described iROC approach [18]. Although some trends can be observed, these are overall all well within the standard deviation of the data, and in general all methods perform similarly at this level of NUS (see Table 3). The linearly sampled data show the narrowest line width at 11 Hz which can be considered the maximum attainable when sampling 512 data points on the constructed Nyquist grid (∼2.7 × T_2). The other methods are all exponentially weighted and result in signal broadening since the missing data are set to "0" (and not reconstructed). The variation in linewidth between the different sampling methods are also within the statistical error of the data.

3.3. Bursts in 2D

In two dimensions, the added degree of freedom greatly expands the possible arrangement of bursts. Using the algorithm described it is possible to organize samples as being part of a burst in one or two dimensions. The burst length may the same or different in each dimension. In this section, we explore some of the possible permutations in 2D by plotting the PSF of a number of 2D sampling schedules with different geometrical clustering of points, with and without jittering (see Figs. 4 and 5). In each case 512 samples are drawn from a 64 × 128 grid (6.25%).

The extension of clustering in 2D to additional dimensions will follow the same trends and is not further explored here, however, we note that the software implementation of the algorithm does allow for up to 3 NUS dimensions.

Table 3
Summary of results from the automated peak picking by Peaky from simulated spectral data generated using different sampling methods. Linear sampling refers to sampling of 512/512 data points, all other data were generated by sampling 128/512 points. See text or Table 1 heading for details of abbreviations used. Recovery rate is the fraction of synthetic input signals detected (out of 7). False discovery rate is ratio of the number of artifacts identified and the total number of signals detected, at a threshold level required to detect at least 7 peaks. Frequency error and average linewidths (full width at half maximum) are also reported (in Hz).

	Recovery rate		False discovery rate		Frequency error [Hz]		Average LW [Hz]	
	Av	St. dev.	Av	St. dev.	Av	St. dev.	Av	St. dev.
Linear	1	0	0	0	0.09	0.03	11.09	0.11
ERS	9.999E−01	4.5E−03	8.7E−03	4.4E−02	0.92	0.31	19.6	2.2
ERS ^2c	9.990E−01	1.2E−02	1.4E−02	5.6E−02	0.90	0.32	19.4	2.3
ERS $^2cf_{0.25}$	9.997E−01	6.4E−03	8.0E−03	3.9E−02	0.89	0.30	19.2	2.1
ERS $^2cf_{0.5}$	9.996E−01	7.8E−03	8.9E−03	4.1E−02	0.87	0.31	18.9	2.1
ERS $^2cf_{0.75}$	9.999E−01	4.5E−03	5.0E−03	2.9E−02	0.82	0.26	18.2	1.8
ERS ^3c	9.986E−01	1.4E−02	1.8E−02	6.1E−02	0.92	0.33	19.4	2.5
ERS $^3cf_{0.25}$	9.997E−01	6.4E−03	8.0E−03	4.5E−02	0.85	0.29	18.7	1.9
EJS	9.994E−01	9.0E−03	6.3E−03	3.2E−02	0.89	0.30	19.3	1.4
EJS ^2c	9.997E−01	6.4E−03	9.8E−03	4.2E−02	0.90	0.32	19.1	1.8
EJS $^2cf_{0.25}$	9.999E−01	4.5E−03	8.0E−03	3.7E−02	0.90	0.31	19.2	2.0
EJS $^2cf_{0.5}$	9.999E−01	4.5E−03	6.8E−03	3.8E−02	0.87	0.29	19.0	1.8

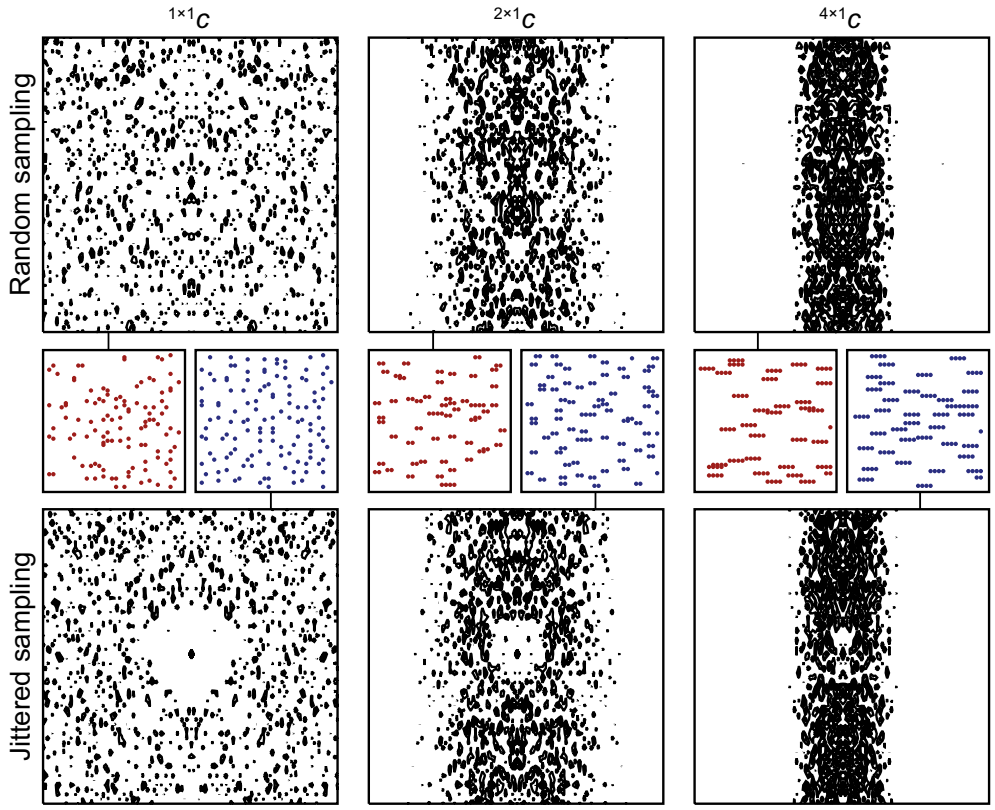

Fig 4. Point-spread function of different sampling methods evaluated here. The top row shows PSFs derived from sampling distributions where 512 samples are drawn randomly from a weighted probability-density function spanning a 64 × 128 grid (6.25%). The bottom row shows the corresponding PSFs where the samples are drawn from equiprobable regions (jittered sampling/quantile sampling). The middle row shows a region (first half of the grid in each dimension) of the sampling coordinates (the origin is at the bottom left) for each PSF (as indicated by the connecting lines). The three columns represent different burst patterns, as indicated in the column headings according to the nomenclature introduced in the theory and methods section.

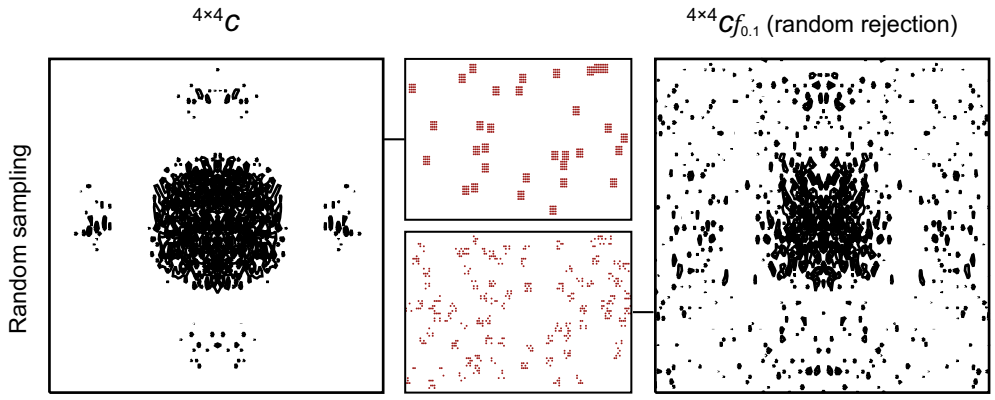

Fig. 5. Point-spread function (PSF) of random sampling with bursts along two dimensions. The left image shows the PSF corresponding to data sampled in bursts of length 4 along each dimension (on the Nyquist grid), and the right images shows the PSF of the same number of samples but where each 4 by 4 burst is sampled nonuniformly. The corresponding sampling coordinates are shown in the middle column (as indicated by the connecting line).

3.4. Experimental data

The application of the clustered sampling method to experimental data was investigated using a ^{15}N-NOESY spectrum. The red shift (to lower frequencies) of the sampling noise should in principle concentrate the sampling artifacts near the strong diagonal peaks, reducing the amount of sampling artifacts near the much weaker off-diagonal signals. In the first instance, ∼30% NUS (748/2500 hyper-complex data points) was applied, where the data were distributed using a variety of sampling methods, including different burst behaviour generated by our clustered sampling method (note that in all cases the $R'(\boldsymbol{K})$ measure for each sampling schedule was monitored to maintain the same inherent sensitivity across all NUS methods compared – this also applies to all subsequent comparisons involving this dataset). This level of NUS is conservative and often applied to complex spectra such as NOESY spectra [19]. In these experiments, the data were reconstructed using maximum entropy reconstruction using an automated parameter selection method (SHARP) [20]. The outcome of this experiment shows that spectral reconstructions of the NUS

data (at 30% NUS) are nearly indistinguishable from each other, and indeed the fully sampled data (Fig. 6). This would suggest that the reconstruction algorithm is very effectively deconvolving the reconstruction artifacts regardless of their PSFs.

The contribution of the sampling noise can be observed by producing the nuDFT spectrum (where the sample points not included in the sampling list are set to 0). Here, we can clearly see that the clustering method is having the expected effect of shifting the sampling artifacts away from the off-diagonal signals (Fig. 7), whereas random sampling results in a more random distribution of these artifacts.

Given that the MaxEnt reconstruction algorithm effectively removed the sampling noise for all NUS sampling methods compared in Fig. 6, regardless of the distribution of the sampling, we sought to increase the level of sampling noise present by reducing the number of points sampled. This was done gradually from 30% NUS, and at ~6% NUS (152/2500) some clear differences emerge (Fig. 8).

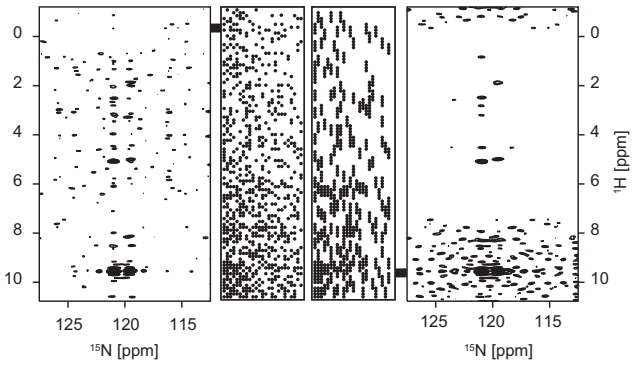

Fig. 7. The DFT of the zero-augmented data (nuDFT), where data points not sampled are set to 0. The corresponding sampling coordinates are shown for the two cases, and connected to the corresponding nuDFT spectrum. Both sampling methods cover 30% of the sampling space and the spectrum on the left is the result of samples drawn randomly from an exponentially weighted probability density function. The spectrum on the right shows the result of sampling in bursts of 4 points along the indirect ^{1}H dimension, where the bursts are selected randomly from a weighted probability density function.

4. Discussion

Here, we have described a new method for nonuniform sampling of multidimensional NMR data. The purpose of this work has been to provide a more solid basis for discussion of the effect of "bursts" of samples that naturally occur in NUS. A method is presented that generates "bursty" NUS data, where the amount of "burstiness" can be controlled. We refer to this mode of sampling as clustered sampling, and the length of the bursts can be specified along each NUS dimension. We have also described a measure of burstiness, allowing better quantitation of this property in future studies.

Further, we have conducted an initial evaluation of the properties of spectral data generated from NUS data containing bursts of samples. The results show that the presence of bursts leads to reduced sampling related noise at a frequency away from the central signal component, which is related to the length of the burst (at subharmonic frequencies of the bandwidth). Bursts of length 2, lead to artifact suppression at $^{1}/_{2}$ SW, bursts of length 3, lead to artifact suppression at $^{1}/_{3}$ SW, etc.

In the PSF, the zero-frequency component corresponds to the integral of samples in the time domain having a non-zero value (i.e. where sampled data points are set to 1 and omitted data set to 0). Thus, if the number of sampled points (set to 1 in the time-domain) is kept constant, on a defined Nyquist grid, the amplitude of the zero-frequency signal will remain constant,

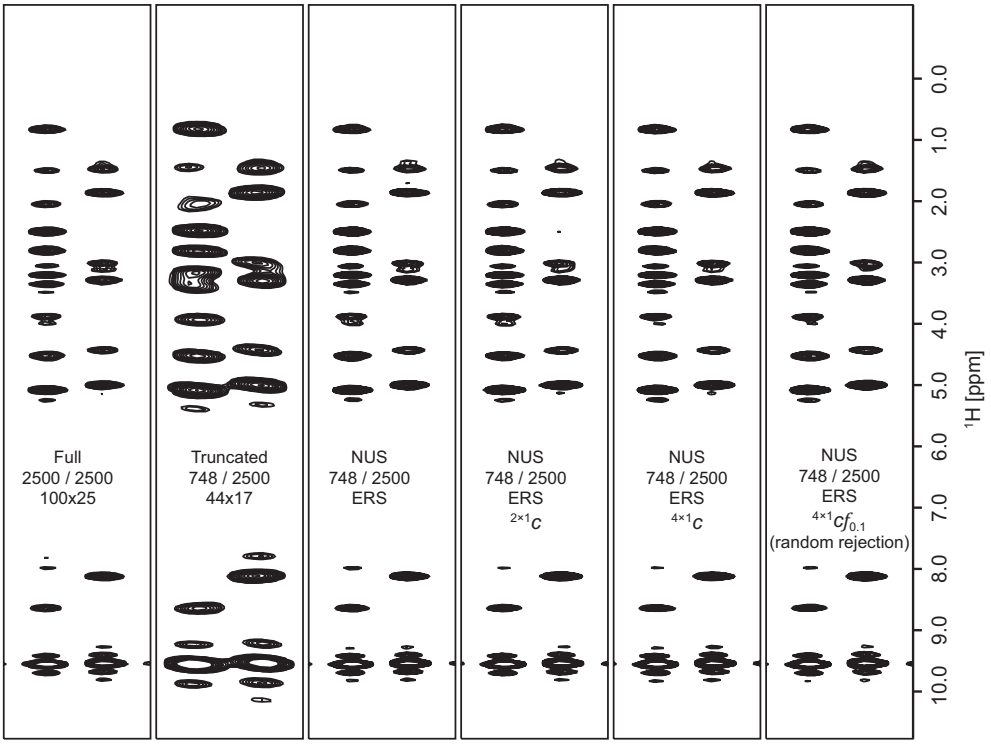

Fig. 6. Maximum entropy spectral reconstruction of a 3D ^{15}N-NOESY dataset. The two columns in each strips correspond to the backbone amides of residues C16 and K10 (left to right) of a 4 kDa peptide (VST×1 – BMRB:25568). The two indirectly sampled dimensions are shown (^{1}H on the y-axis and ^{15}N on the x-axis). The different strips show different sampling regimes. The sampling method is provided on the image using the nomenclature described in the text (see also heading of Table 1). Only samples along the indirect ^{1}H dimension (y-axis) were sampled in bursts.

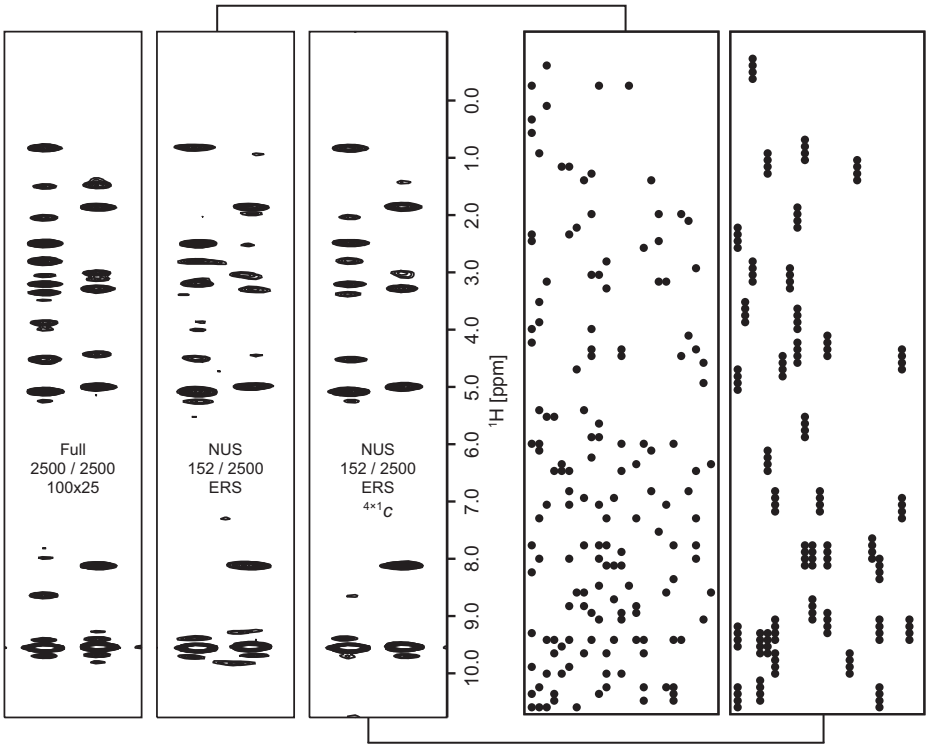

Fig. 8. Maximum entropy spectral reconstruction of a sparsely sampled 3D NOESY experiment (same experimental data as used in Fig. 6/7). The different strips show different sampling regimes. The sampling method is provided on the image using the nomenclature described in the text (see also heading of Table 1). The sampled coordinates are shown on the two right-hand strips and the connecting lines indicate the corresponding spectral reconstruction resulting from those samples. In both cases 6% (of the available data points) is sampled.

regardless of the distribution of the samples. Under these conditions, suppression of artifacts (defined as non-zero frequency signals) in one part of the spectrum naturally leads to increase of sampling artifacts elsewhere (due to Parceval's theorem). In the case of burst sampling these artifacts are shifted to frequencies near the central (zero-frequency) component of the PSF (red-shifted noise). It is worth noting that (i) burst sampling can be viewed as multiplication of a series of box-functions with the time-domain data and (ii) in the extreme case of one long burst, the sampling is equivalent to truncation and zerofilling. The outcome of truncation is very well documented and understood in the NMR literature, and leads to the familiar artifacts often termed truncation artifacts or sinc wiggles [21,22]. It is therefore not surprising to see the red-shift of the sampling noise (and the oscillatory behaviour), as this will eventually lead to truncation artifacts – which perhaps should more generally be considered red-shifted sampling noise.

We note that the red-shifted sampling noise is in direct contrast to artifacts that arise when using methods that seek to evenly distribute the data, which result in blue-shifted sampling noise [4,17]. This led us to explore a potential combination of our clustered sampling method with a jittered-sampling method, and we find the effects to be additive, i.e. artifact reduction near the central frequency component due to jittered sampling, and artifact reduction at a frequency related to the burst length used. This is an interesting outcome as the presence of two regions with reduced artifacts naturally leads to further increase of artifacts elsewhere (again due to the conservation of power between domains).

Next, we compared the outcome of our clustered sampling method to other sampling methods, to explore the consequences of the presence of bursts. There are, however, currently no measures of burstiness for NUS in NMR, hampering quantitation. Considering that the burstiness of sampling schedules has been discussed in the literature on several occasions, it is somewhat surprising that no measure of this property has been put forward. To address this, we developed an algorithm that applies a moving mask with a specified geometry, to assess if a point can be considered to be in a burst of that size. The occupancy of the mask for each point is evaluated and an overall burstiness score is reported.

Together with the burstiness measure, a number of other statistics related to the sampling schedules were determined. Firstly, we ensured that the inherent sensitivity of the sampling schedule ($R'(\boldsymbol{K})$) was kept constant, this allows for an unbiased comparison of the different methods [4,14,23,24]. We find that random sampling tends to result in more bursty sampling than jittered sampling. This is not surprising considering that the jittering approach would seek to maximize the distance between adjacent points (closer to Poisson distribution). The random rejection method developed to reduce the number of bursts, appears to also have the intended outcome as measured by our burstiness metric.

The PSF associated with the different sampling schedules was also produced and statistics relating to these determined. There are no clear synergies in combining the clustered sampling method with the jittered sampling method. Statistical studies of the PSF can be useful but ultimately the performance of these schedules on FIDs will provide a better indicator of performance. For this purpose, we generated a large dataset of synthetic data, where signals of varying intensity and frequency were used as input, and the nuDFT spectrum was evaluated by an automated peak analysis algorithm to yield peak tables that are suitable for assessing the performance of the different sampling methods – in analyses similar to the described iROC approach [18]. In this study, the schedules and the signal frequencies were varied randomly for statistical analysis of the output. Interestingly, we find no clear differences in any of the measured metrics for any of the compared methods. There are trends that suggest that the detection rate

decreases in the presence of bursts, however, conversely the results show that the linewidths trend towards narrower lines for these data (so the result might be due to subtle difference in inherent sensitivity [23]). The most important factor here is likely the inherent sensitivity of the sampling schedules ($R'(\boldsymbol{K})$), and this is by design constrained to be the same for all methods. Thus, one interpretation of this outcome is that, at the level of NUS used, the distribution of the NUS data is not critically important if the inherent sensitivity of the different sampling methods is kept constant. This conclusion is only valid for cases where a significant proportion of the time domain has been sampled (128/512 samples). Although, it is tempting to explore how these relationships are affected by changes in the skew of the sampling (e.g. sine weighting), dimensionality, level of NUS (e.g. 5%, 10%, 15%, 20%, etc.) or number of synthetic signals and their dynamic range etc., these studies are beyond the scope of this work and form the basis for future investigations. To explore the implementation of the clustered sampling method in multiple dimensions, we also explored a limited number of 2D NUS scenarios, and found that overall, these follow the same trends as those seen in 1D.

The observation that the presence of bursts in the sampling schedule results in sampling noise near the signals giving rise to them, raises the question of whether this mode of sampling may be of particular benefit when applied to cases where strong diagonals may yield strong off-diagonal sampling artifacts that might obscure weak spectral features. This includes important experiments commonly used in assessing protein structures, such as NOESY and TOCSY spectra. 3D versions of these experiments are commonly used in protein structure determination of isotope labeled samples and are currently the most time-intensive experiments in routine structural studies [25]. Here, we introduced bursts in the indirect ^{1}H dimension of a 3D (^{15}N)-NOESY-HSQC. Since we are not concerned with comparing methods of spectral reconstruction, we simply ensured that the parameter selection, in the maximum entropy reconstruction method used, allowed for qualitative comparisons [14,20]. (A more comprehensive comparison of reconstruction methods is pursued elsewhere [13] and is outside the scope of our work.) Although, clear gains in resolution can be seen when applying NUS compared to truncation of the data, there is no compelling difference between the different sampling methods at high levels of NUS coverage. This is consistent with the observation in 1D where, at high levels of NUS the distribution of the NUS data appears to have little effect on the outcome. Thus, although there are clear differences in the distribution of the sampling noise (Fig. 7), these are effectively deconvolved by the reconstruction algorithm [26].

To explore if any differences emerge with reduced levels of NUS, we monitored the spectral quality as a function of NUS percentage, comparing our clustered sampling method with time-equivalent randomly sampled data (again in all cases the inherent sensitivity is kept constant). Interestingly, it is only at very low levels of NUS that we start to see clear differences between the two sampling methods (Fig. 8).

We note that this is well below what is commonly recommended for such complex data and these observations suggest that any benefits associated with bursty sampling may only prove beneficial in extreme cases of NUS [25]. It is also worth noting that the compression of the data at 30% NUS corresponds to reducing the experiment time from ~28 h to 8.5 h, and further reduction to 6% would yield a 3D NOESY dataset in less than 2 h. Although, a very impressive outcome, in practical terms the additional ~7 h of time savings are unlikely to motivate the NOE losses seen at these low levels of sampling (Fig. 8). Nevertheless, there are numerous instances where maximum compression is required, examples include (i) studies of kinetic processes by multidimensional data [27], (ii) studies of unstable proteins [20] or (iii) when data is analyzed during acquisition (e.g. targeted acquisition) [28]. It is under these circumstances where further exploration of bursts is likely to prove most beneficial.

5. Conclusions

Here we have described a framework for producing and quantitating random sampling where the data appear in bursts. This framework will be useful for further exploration of this novel mode of sampling in multidimensional NMR, and a more solid foundation for discussing the appearance of bursts as a general phenomenon in nonuniform sampling. Systematic introduction of bursts of predefined length, produces a characteristic point-spread-function with red-shifted sampling noise. A systematic analysis of 1D data, shows that at high levels of sampling coverage (25%), there is no apparent advantage of introducing bursts when compared to random sampling (given that the inherent sensitivity of the sampling is maintained). The observations in 1D, are extended to 2D using a limited number of examples. We find that presence of bursts may have particular benefits when applied to data acquisition of NOESY type spectra (in particularly in ^{15}N-NOESY data) where the red-shifted noise, reduces interference of artifacts arising from the strong diagonal signals with the much weaker off-diagonal cross-peaks. At a conservative level of under-sampling (30%) there are no clear advantages observed, however, some improvements are observed when the number of sampled points is significantly reduced (6%).

Acknowledgements

MM acknowledges financial support from the Australian Research Council (DP140101098) and the University of Queensland (UQ Developmental Research Fellowship). TMM acknowledges financial support from the UQ Research Training Program, funded by the Commonwealth Government of Australia. The authors are grateful to assistance from the NMRBox team (Prof. Hoch, Dr Maciejewski and Mr Weatherby at UConn Health Centre), for hosting the software implementation of the algorithms presented.

References

[1] M. Mobli, J.C. Hoch, Nonuniform sampling and non-Fourier signal processing methods in multidimensional NMR, Prog. Nucl. Magn. Reson. Spectrosc. 83 (2014) 21–41.
[2] J.C.J. Barna, E.D. Laue, M.R. Mayger, J. Skilling, S.J.P. Worrall, Exponential sampling, an alternative method for sampling in two-dimensional Nmr experiments, J. Magn. Reson. 73 (1987) 69–77.
[3] M. Mobli, A.S. Stern, J.C. Hoch, Spectral reconstruction methods in fast NMR: reduced dimensionality, random sampling and maximum entropy, J. Magn. Reson. 182 (2006) 96–105.
[4] M. Mobli, Reducing seed dependent variability of non-uniformly sampled multidimensional NMR data, J. Magn. Reson. 256 (2015) 60–69.
[5] D.L. Craft, R.E. Sonstrom, V.G. Rovnyak, D. Rovnyak, Nonuniform sampling by quantiles, J. Magn. Reson. 288 (2018) 109–121.
[6] B. Worley, R. Powers, Deterministic multidimensional nonuniform gap sampling, J. Magn. Reson. 261 (2015) 19–26.
[7] S.G. Hyberts, K. Takeuchi, G. Wagner, Poisson-gap sampling and forward maximum entropy reconstruction for enhancing the resolution and sensitivity of protein NMR data, J. Am. Chem. Soc. 132 (2010) 2145–2147.
[8] A.D. Schuyler, M.W. Maciejewski, H. Arthanari, J.C. Hoch, Knowledge-based nonuniform sampling in multidimensional NMR, J. Biomol. NMR 50 (2011) 247–262.
[9] M.W. Maciejewski, H.Z. Qui, I. Rujan, M. Mobli, J.C. Hoch, Nonuniform sampling and spectral aliasing, J. Magn. Reson. 199 (2009) 88–93.
[10] I.E. Ndukwe, A. Shchukina, K. Kazimierczuk, C. Cobas, C.P. Butts, EXtended ACquisition Time (EXACT) NMR-A Case for 'Burst' Non-Uniform Sampling, ChemPhysChem 17 (2016) 2799–2803.
[11] C.H.Y. Lau, G.F. King, M. Mobli, Molecular basis of the interaction between gating modifier spider toxins and the voltage sensor of voltage-gated ion channels, Sci Rep-Uk 6 (2016) 34333.
[12] M. Mobli, A.S. Stern, W. Bermel, G.F. King, J.C. Hoch, A non-uniformly sampled 4D HCC(CO)NH-TOCSY experiment processed using maximum entropy for rapid protein sidechain assignment, J. Magn. Reson. 204 (2010) 160–164.

[13] M.W. Maciejewski, A.D. Schuyler, M.R. Gryk, I.I. Moraru, P.R. Romero, E.L. Ulrich, H.R. Eghbalnia, M. Livny, F. Delaglio, J.C. Hoch, NMRbox: a resource for biomolecular NMR computation, Biophys. J . 112 (2017) 1529–1534.
[14] S. Paramasivam, C.L. Suiter, G. Hou, S. Sun, M. Palmer, J.C. Hoch, D. Rovnyak, T. Polenova, Enhanced sensitivity by nonuniform sampling enables multidimensional MAS NMR spectroscopy of protein assemblies, J. Phys. Chem. B 116 (2012) 7416–7427.
[15] J.J. More, D.C. Sorensen, B.S. Garbow, K.E. Hillstrom, MINIPACK PROJECT, Sources Dev Math Software (1984) 88–111.
[16] R.A. Chylla, J.L. Markley, Theory and application of the maximum likelihood principle to NMR parameter estimation of multidimensional NMR data, J. Biomol. NMR 5 (1995) 245–258.
[17] K. Kazimierczuk, A. Zawadzka, W. Kozminski, Optimization of random time domain sampling in multidimensional NMR, J. Magn. Reson. 192 (2008) 123–130.
[18] M.A. Zambrello, M.W. Maciejewski, A.D. Schuyler, G. Weatherby, J.C. Hoch, Robust and transferable quantification of NMR spectral quality using IROC analysis, J. Magn. Reson. 285 (2017) 37–46.
[19] B. Mohanty, M.L. Williams, B.C. Doak, M. Vazirani, O. Ilyichova, G. Wang, W. Bermel, J.S. Simpson, D.K. Chalmers, G.F. King, M. Mobli, M.J. Scanlon, Determination of ligand binding modes in weak protein-ligand complexes using sparse NMR data, J. Biomol. NMR 66 (2016) 195–208.
[20] T. Miljenović, X. Jia, P. Lavrencic, B. Kobe, M. Mobli, A non-uniform sampling approach enables studies of dilute and unstable proteins, J. Biomol. NMR 68 (2017) 119–127.
[21] M. Mobli, J.C. Hoch, G.F. King, Fast acquisition methods in multidimensional NMR, in: A.J. Dingley, S.M. Pascal (Eds.), Advances in Biomedical Spectroscopy, IOS Press, 2011, pp. 305–337.
[22] J. Keeler, Elimination of truncation artifacts from NMR spectra. Application to carbon-13 multiplicity determination by two-dimensional spectroscopy, J. Magn. Reson. 56 (1984) (1969) 463–470.
[23] D. Rovnyak, M. Sarcone, Z. Jiang, Sensitivity enhancement for maximally resolved two-dimensional NMR by nonuniform sampling, Magn. Reson. Chem. 49 (2011) 483–491.
[24] M.R. Palmer, B.R. Wenrich, P. Stahlfeld, D. Rovnyak, Performance tuning non-uniform sampling for sensitivity enhancement of signal-limited biological NMR, J. Biomol. NMR 58 (2014) 303–314.
[25] T.M. Miljenović, X. Jia, M. Mobli, Nonuniform sampling in biomolecular NMR, in: G.A. Webb (Ed.), Modern Magnetic Resonance, Springer International Publishing, Cham, 2018, pp. 2035–2054.
[26] M. Mobli, A.S. Stern, J.C. Hoch, Chapter 9 Maximum Entropy Reconstruction, in: Fast NMR Data Acquisition: Beyond the Fourier Transform, The Royal Society of Chemistry, 2017, pp. 252–266.
[27] P. Giraudeau, L. Frydman, Ultrafast 2D NMR: an emerging tool in analytical spectroscopy, Annu. Rev. Anal. Chem. 7 (2014) 129–161.
[28] V.A. Jaravine, V.Y. Orekhov, Targeted acquisition for real-time NMR spectroscopy, J. Am. Chem. Soc. 128 (2006) 13421–13426.